Chapter 5

Self-assembly of BChl *c* in chlorosomes of the green sulfur bacteria *C. tepidum*: a comparison between the *bchQR* mutant and the wild-type

The self-aggregated state of BChl *c* in chlorosomes belonging to a BChl biosynthesis double mutant *bchQR* of the green sulfur bacteria *C. tepidum*, which produces a single 17^2-farnesyl-*R*-[E,M] BChl *c* homologue, was characterized by MAS dipolar homonuclear ^{13}C-^{13}C and heteronuclear ^{1}H-^{13}C correlation spectroscopy. Well resolved datasets with ^{13}C linewidths of 200-300 Hz and ^{1}H linewidths of 1.7-2.0 kHz, were collected from ^{13}C enriched *bchQR* chlorosome preparations, reflecting a homogeneously ordered state of the BChl *c* in the sample. A near complete ^{1}H and ^{13}C chemical shift assignment has been obtained. Pronounced doubling (1:1) of selective ^{13}C and ^{1}H resonances is observed, at the 3^1-C/3^1-H, 5-C/5-H, 7^1-H_3, 13^1-C, 14-C, and 17-C/17-H positions of the BChl *c* ring, revealing the presence of two distinct and nonequivalent BChl *c* components. Distance constraints that were resolved point to *syn-anti* stacking of the BChl *c* molecules. *Syn* and *anti* coordination can give rise to different degrees of ring deformation in BChl *c*, primarily of the saddling, ruffling, and doming types. Chemical shift calculations were performed on *syn* and *anti* coordinated monomers of BChl *c* that were optimized individually and taken from a larger optimized aggregate. These calculations suggest that the different ring deformations that arise from the steric hindrance of the methyl group present at the 20-meso position upon rotation of the methyl group at 3^1-C going from a *syn* to an *anti* coordinated molecule within a stack is in part responsible for the doubling observed in the NMR spectra.

5.1 Introduction

An in depth combined solid-state NMR, cryo-EM and DFT based investigation of chlorosomes from the *bchQRU* mutant described in Chapter 4 has led to its detailed microstructure and suprastructure in which the chlorosomal tubules are shown to be built from *syn-anti* parallel stacks having alternating molecular conformations of the 3^1-C side chain [1-3]. In the *bchQRU* mutant there is quasi-symmetry around each BChl, and there is no pronounced splitting of signals in the NMR. In this Chapter, the structure of chlorosomes from the *bchQR* double mutant of *C. tepidum* is characterized, which is thought to be closer to the WT than the *bchQRU* species, since it produces chlorosomes containing almost 100% of a single 17^2-farnesyl-*R*-[E,M] BChl *c* homologue, in contrast with the 17^2-farnesyl-*R*-[E,M] BChl *d* synthesized by the *bchQRU* strain [4,5]. An advantage in studying this mutant in addition to the WT is the increased spectral resolution that is attained due to the pigment homogeneity in the *bchQR* chlorosomes [1,2,6]. Using uniformly ^{13}C and ^{15}N enriched preparations of the *bchQR* and WT chlorosomes for solid-state NMR analyses; we were able to directly determine distance constraints from the resulting high resolution data allowing the determination of a *syn-anti* based microstructure for the *bchQR* chlorosomes.

The chlorosomes of the *bchQR* mutant give two sets of NMR peaks, similar to WT chlorosomes, at specific positions on the BChl *c* ring [6,7]. The two fractions are of almost equal intensity, unlike in the chlorosomes from the *bchQRU* mutant, where one set of signals strongly dominates over the other, and in the WT, where the ratio is ~7:3 [6,7]. Out-of-plane deformations arising from *syn* and *anti* coordination of BChl *c* were calculated using the normal-coordinate structural decomposition method [8,9]. *Syn* and *anti* coordination gave rise to varying degrees of deformation of the saddling, ruffling, and doming type. DFT based chemical shift calculations performed on *syn* and *anti* coordinated monomers of BChl *c* taken from a larger optimized aggregate show that the ring deformation arising from the methyl group present at the 20-meso position, as well as the alternating 3^1-C molecular conformation arising from the *syn-anti*

structure, are in part responsible for the doubling observed in the NMR spectra of the *bchQR* mutant.

5.2 Experimental section

Cells of *C. tepidum* WT and the *bchQR* double mutant strain described in Gomez *et al.* were grown as described in Balaban *et al.* [2,10]. The preparation of ^{13}C-^{15}N enriched chlorosomes and the isolation of BChl *c* is described previously [10].

2D ^{13}C-^{13}C RFDR, ^{1}H-^{13}C FSLG and ^{13}C-^{13}C CHHC NMR datasets were acquired with a Bruker DSX-750 spectrometer at sample temperatures of 277K as described in Chapter 4, for chlorosomes from the WT and from the *bchQR* mutant of *C. tepidum* [11-14]. 1D ^{15}N CP-MAS experiments were performed with CP periods of 5.12 ms. RFDR spectra were recorded with mixing times of 1.4 and 2.9 ms. The ^{13}C and ^{1}H shifts in solution ($\sigma_{liq}^{C}, \sigma_{liq}^{H}$), were determined with 2D ^{13}C-^{13}C COSY, ^{1}H-^{1}H COSY and ^{1}H-^{13}C HSQC NMR spectra of the BChl *c* monomer in CD_2Cl_2 with 5% CD_3OD recorded on a DMX-600 spectrometer (Bruker, Karlsruhe, Germany).

The DFT based chemical shift calculations are performed as described in Chapter 4 [15-22]. The six out-of-plane normal deformations of the saddling (sad, B_{2u}), ruffling (ruf, B_{1u}), doming (dom, A_{2u}), waving (wav(x), wav(y); E_g), and propellering (pro, A_{1u}) type were calculated for optimized BChl *c* monomers in the lowest frequency mode using the NSD program available online developed in the group of Shelnutt and co-workers [8,9].

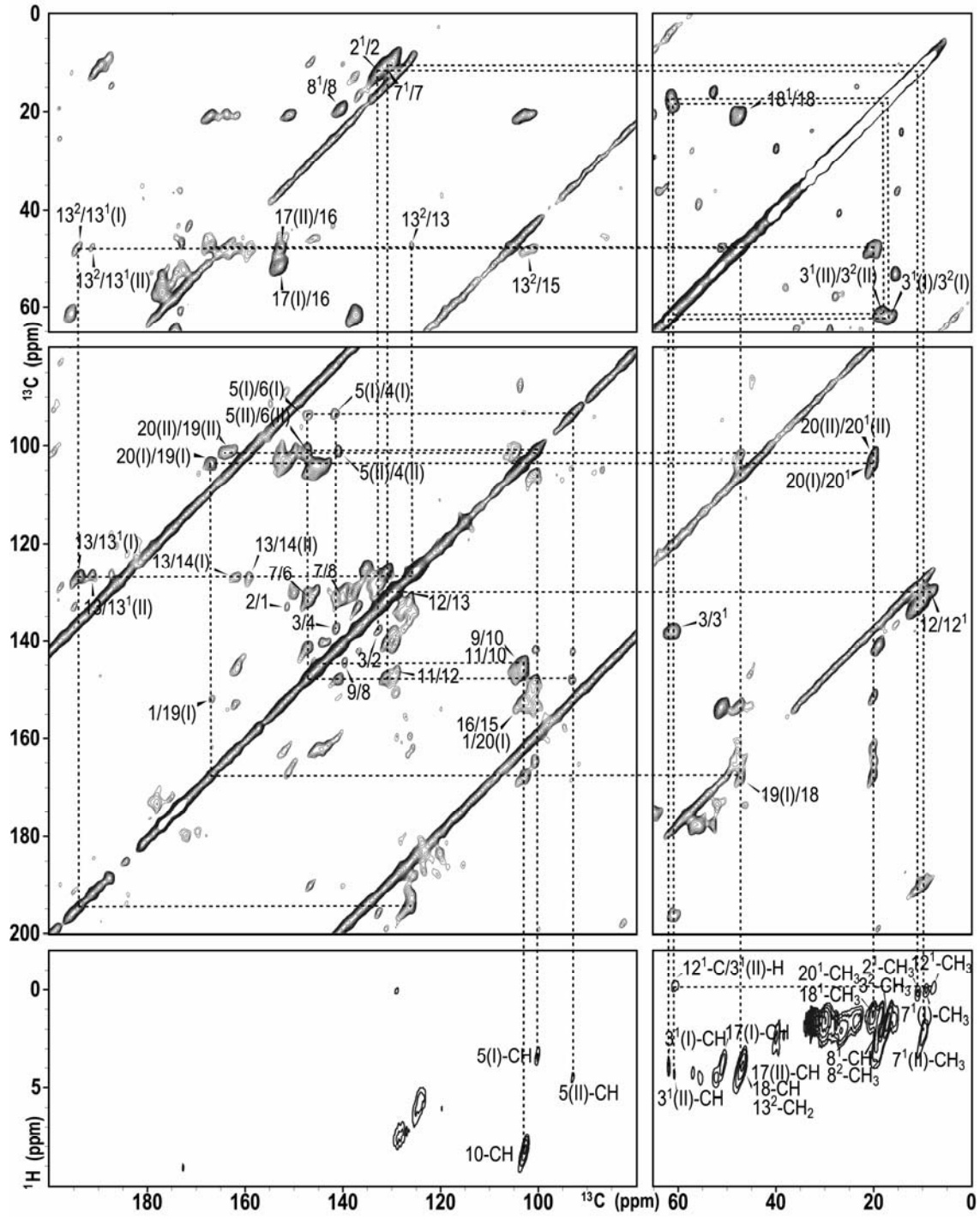

Figure 5.1 Contour plot sections of a ^{13}C-^{13}C MAS NMR dipolar correlation spectrum of chlorosomes from the *bchQR* mutant recorded in a field of 17.6 T using a spinning frequency of 11 kHz and a mixing time of 1.4 ms. The lower panels show contour plot sections of an ^{1}H-^{13}C MAS NMR FSLG dipolar correlation spectrum recorded in the same field employing a spinning rate of 13 kHz. The FSLG panels are plotted at different contour levels. The ^{13}C-^{13}C and ^{1}H-^{13}C connectivity networks are indicated with dashed lines, and the two spectral components are numbered I and II.

5.3 Results and discussion

5.3.1 Chemical shift assignment

The ^{13}C and ^{1}H chemical shift assignment of the chlorosomes from the *bchQR* mutant is obtained from the well resolved two-dimensional homonuclear ^{13}C-^{13}C and heteronuclear ^{1}H-^{13}C dipolar correlation datasets shown in Figure 5.1. The nearest-neighbor connectivity of the molecular network leading to the assignment of BChl *c* in chlorosomes is indicated with dashed lines. The lines are very narrow, of the order of 1-2 ppm, which is attributed to the increased order of the supramolecular arrangement of the BChl molecules in the *bchQR* mutant relative to the WT, which is in turn attributed to the presence of a single 17^2-farnesyl-*R*-[E,M] BChl *c* homologue. The RFDR spectra recorded for the chlorosomes from the WT of *C. tepidum* with mixing times of 1.4 and 2.9 ms have a better resolution than previously reported data measured at a lower field [10,23]. The resolution of the data collected from *bchQR* chlorosomes remains superior, however, and reveals a better microscopic order and probably tighter packing in the mutant chlorosomes relative to the WT. The ^{13}C chemical shift assignment for chlorosomes from the WT agrees with the data reported by Balaban and co-workers [10].

For chlorosomes from the *bchQR* mutant two components are observed for specific ^{13}C resonances, at positions 3^1-C, 3^2-C, 4-C, 5-C, 6-C, 7-C, 7^1-C, 13^1-C, 14-C, 17-C, 19-C, and 20-C of the BChl *c* ring and are denoted as components I and II. Corresponding ^{1}H resonances in the ^{1}H-^{13}C spectrum at the 3^1-H, 5-H, 7^1-H_3 and 17-H positions also give two signals. For the WT two components are observed for ^{13}C resonances at all but the 13^1-C, 14-C, and 20^1-C positions seen for the *bchQR* mutant, while additional doubling is observed at positions 8-C and 16-C. The differences in ^{1}H chemical shifts between components I and II are generally less than 1 ppm except for 7^1-H_3 (2-4 ppm), and are small compared to the differences of 2-5 ppm in their ^{13}C chemical shifts. The ^{13}C chemical shift assignment of components I and II for chlorosomes from the *bchQR* mutant and the WT have been listed in Table 5.1 and the difference in chemical shifts between the components has been plotted in Figures 5.3A

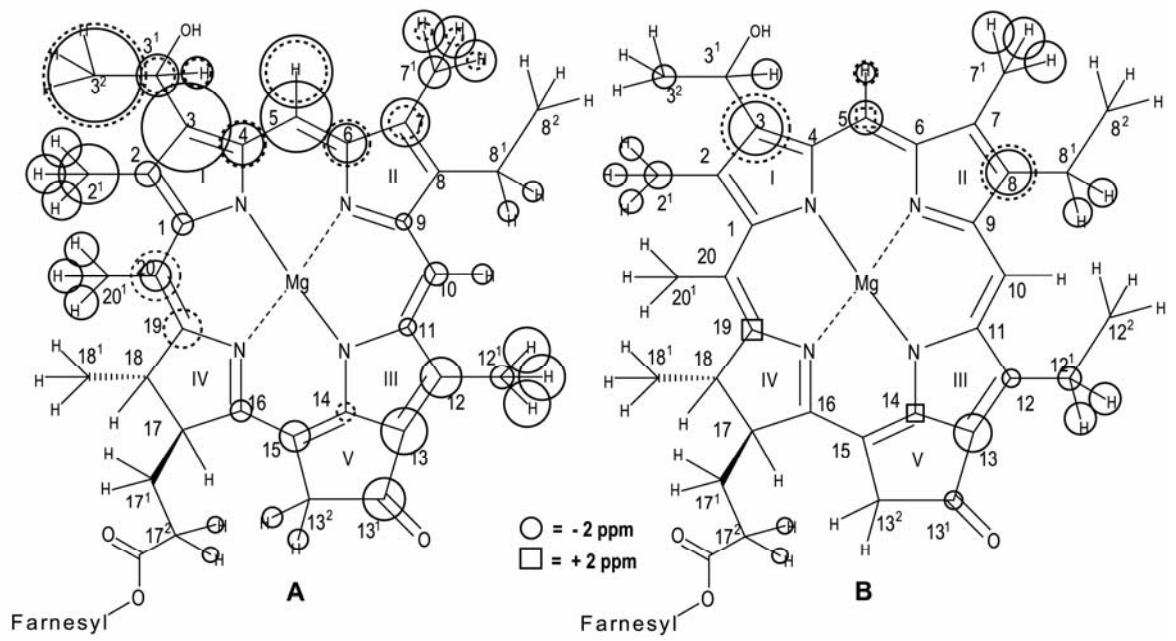

Figure 5.2 Observed ^{1}H and ^{13}C aggregation shifts of chlorosomes from the (A) *bchQR* mutant and (B) WT of *C. tepidum* are shown for values ≥ |±1.5| ppm. The aggregation shifts of components I and II are plotted as dark and dashed circles respectively. The size of the circle/square is proportional to the magnitude of the shift.

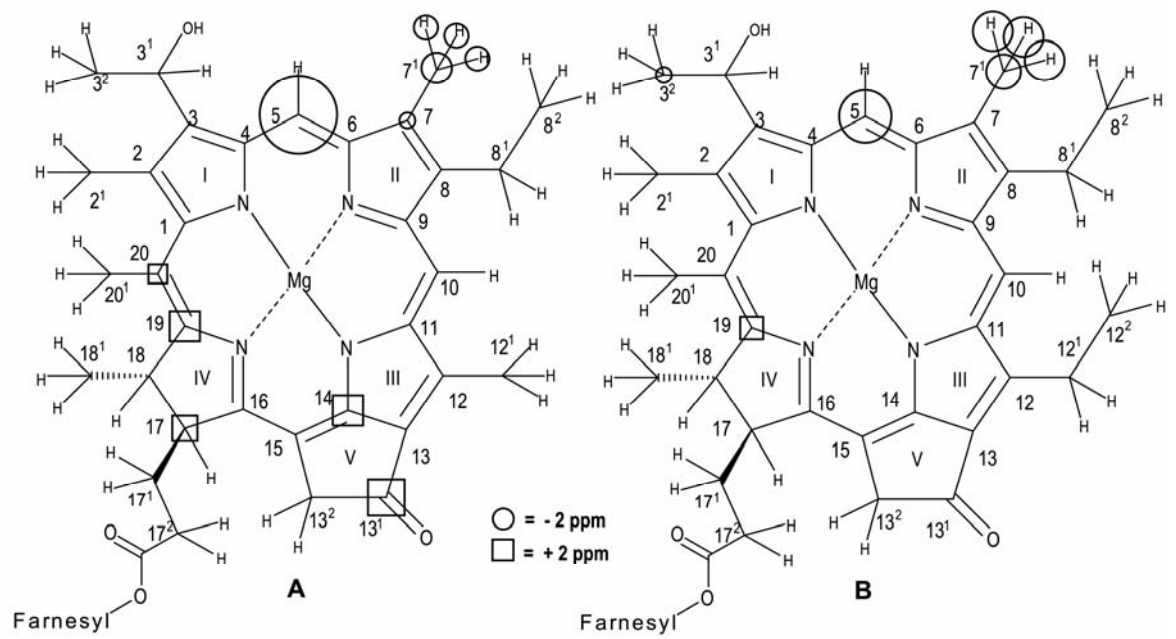

Figure 5.3 The difference in ^{13}C chemical shifts between the components I and II of the chlorosomes from the (A) *bchQR* mutant and the (B) WT for values $\Delta\sigma_i \geq \pm 1.5$ ppm are indicated. The size of the circle/square is proportional to the magnitude of the shift.

Table 5.1 ^{13}C chemical shifts in ppm of components I (σ_I^C) and II (σ_{II}^C) of BChl *c* from chlorosome of the *bchQR* mutant and the WT and their difference $\Delta\sigma_{I,II}^C = \sigma_I^C - \sigma_{II}^C$.

Position[a]	*bchQR*			WT		
	σ_I^C	σ_{II}^C	$\Delta\sigma_{I,II}^C$	σ_I^C	σ_{II}^C	$\Delta\sigma_{I,II}^C$
3^1	61.4	62.1	-0.7	63.7	63.1	0.6
3^2	17.6	16.7	0.9	23.4	24.9	-1.5
4	141.9	141.5	0.4	144.6	143.9	0.7
5	93.5	100.9	-6.8	97.0	102.0	-5.0
6	147.5	146.8	0.7	149.9	149.5	0.4
7	130	131.5	-1.5	131.9	133.2	-1.3
7^1	7.5	10.4	-2.9	7.7	11.0	-3.3
8	[b]	[b]		139.6	138.3	1.3
13^1	194.8	191.3	3.5	[b]	[b]	
14	162.1	159.2	2.9	[b]	[b]	
16	[b]	[b]		154.1	154.3	-0.2
17	51.3	48.9	2.4	49.0	48.9	0.1
19	167.2	164.3	2.9	169.7	167.5	2.2
20	103.2	101.4	1.8	105	103.7	1.3
20^1	20.7	20.3	0.4	[b]	[b]	

[a] The numbering is according to Figure 5.2. [b] Only a single component seen at that position.

Table 5.2 ^1H solution (σ_{liq}^H) and solid-state chemical shifts (σ_i^H) of component I of BChl *c* chlorosome of the *bchQR* mutant and the WT, as well as aggregation shifts $\Delta\sigma_i^H = \sigma_i^H - \sigma_{liq}^H$ are given in ppm

Position[a]	*bchQR*			WT		
	σ_{liq}^H	σ_i^H	$\Delta\sigma_i^H$	σ_{liq}^H [b]	σ_i^H	$\Delta\sigma_i^H$
5	9.7	2.8	-6.9	9.6	7.8	-1.8
10	9.5	7.6	-1.9	9.4	9.6	0.2
17	4.1	3.2	-0.9	4.1	4.2	0.1
18	4.6	3.3	-1.3	4.5	4.2	-0.3
2^1	3.3	-0.4	-3.7	3.3	1.1	-2.2
3^1	6.3	3.3	-3	6.3	3.5	-2.8
3^2	1.9	1.0	-0.9	2.0	0.8	-1.2
7^1	3.3	-0.6	-3.9	3.2	-0.7	-3.9
8^1	3.7	1.9	-1.9	3.7	1.0	-2.7
8^2	1.7	0.7	-1.0	1.6	[e]	
12^{1c}	3.6	-0.8	-4.4	4.0	1.0	-3.0
12^{2d}				1.8	[e]	
13^2	5.1	3.2	-1.9	5.1	4.5	-0.6
17^1	2.2	0.9	-1.3	2.1	0.9	-1.2
17^2	2.4	0.9	-1.5	3.4	0.9	-1.5
18^1	1.5	0.6	-0.9	1.4	1.1	-0.3
20^1	3.8	0.6	-3.2	3.7	3.0	-0.7

[a] The numbering is according to Figure 5.2. [b] van Rossum *et al.* 2001). [c] 12^1 is CH_3 for the *bchQR* mutant and CH_2 for the WT. [d] 12^2 is CH_3 for the WT. [e] Signals could not be resolved.

and B respectively, where the radius of the circle denotes the magnitude of the difference [24]. The ^{1}H (σ_i^H) and ^{13}C (σ_i^C) shifts of the BChl *c* ring from chlorosomes belonging to the *bchQR* mutant and the WT, following the molecular connectivity network of component I, are summarized in Tables 5.2 and 5.3. The chemical shifts are used to calculate the aggregation shifts $\Delta\sigma_i^C = \sigma_i^C - \sigma_{liq}^C$ and $\Delta\sigma_i^H = \sigma_i^H - \sigma_{liq}^H$ for ^{13}C and ^{1}H. The aggregation shifts for components I and II for chlorosomes from the *bchQR* mutant and the WT have been plotted in Figures 5.2A and B. In the *bchQR* mutant 3^2-C shows an anomalously large aggregation shift of -8.9 ppm which is not mirrored in 3^2-H_3 shifts. The pattern of aggregation shifts for the WT is in agreement with previously reported data [7]. We observe additional upfield shifts at positions 8^1-H_2 and 17^2-H_2, and downfield shifts at positions 14-C and 19-C, for component I of the WT.

Table 5.3 ^{13}C solution (σ_{liq}^C) and solid-state chemical shifts (σ_i^C) of component I of BChl *c* from the *bchQR* and WT chlorosomes as well as their aggregation shifts $\Delta\sigma_i^C = \sigma_i^C - \sigma_{liq}^C$ are given in ppm.

Position[a]	*bchQR*			WT		
	σ_{liq}^C	σ_i^C	$\Delta\sigma_i^C$	σ_{liq}^C [b]	σ_i^C [c]	$\Delta\sigma_i^C$
1	153.6	151.6	-2.0	153.8	153.8	0.0
2	135.3	132.9	-2.4	135.2	134.7	-0.5
3	145.9	137.4	-8.5	145.2	140.1	-5.1
4	145.9	141.9	-4.0	145.3	144.6	-0.7
5	100.3	93.5	-6.8	100.2	97.0	-3.2
6	151.2	147.5	-3.7	150.7	149.9	-0.8
7	134.6	130	-4.6	133.6	131.9	-1.7
8	144.3	140.3	-4.0	143.5	139.2	-4.3
9	145.9	144.4	-1.5	146.1	147.5	1.4
10	105.8	103.6	-2.2	105.6	105.9	0.3
11	147.6	146.0	-1.6	147.7	146.8	-0.9
12	134.0	130.1	-3.9	140.7	139	-1.7
13	131.2	126.8	-4.4	131.0	127.4	-3.6
14	160.9	162.1	1.2	161.1	162.7	1.6
15	105.7	102.8	-2.9	104.9	103.8	-1.1
16	154.5	152.5	-2.0	154.3	154.1	-0.2
17	50.3	51.3	1.0	50.1	49.0	-1.1
18	48.2	47.6	-0.6	48.2	48.3	0.1
19	167.9	167.2	-0.7	167.8	169.7	1.9
20	106.1	103.2	-2.9	104.7	105.0	0.3
2^1	17.0	11.3	-5.7	17.0	14.4	-2.6
3^1	65.4	61.4	-4.0	64.1	63.7	-0.4
3^2	26.5	17.6	-8.9	25.6	23.4	-2.2
7^1	10.5	7.5	-3.0	10.6	7.7	-2.9

Table 5.3 *(continued)*

8^1	19.6	19.2	-0.4	19.2	18.0	-1.2
8^2	17.3	*d*		17.1	*f*	
12^1	12.6	10.4	-2.2	20.8	18.6	-2.2
12^2				16.6	*f*	
13^1	198.8	194.8	-4.0	198.2	196.5	-1.7
13^2	48.7	47.9	-0.8	49.1	49.3	0.2
17^1	30.0	30.4*e*	0.4	29.7	*f*	
17^2	30.1	30.4*e*	0.3	30.7	*f*	
17^3	174.5	*f*		173.7	*f*	
18^1	20.4	20.7	0.3	20.6	21.1	0.5
20^1	21.3	20.3	-1.0	21.1	20.3	-0.8
F1	61.5	*f*		61.3	*f*	
F2	117.5	*f*		117.5	*f*	
F3	143.1	*f*		142.4	139.9	-2.5
F4	39.6	39.8	0.2	39.3	39.4	0.1
F5	26.0	27.4	1.4	26.4	26.5	0.1
F6	124.1	125.0	0.9	123.3	123.7	0.4
F7	135.9	135.3	-0.6	135.1	134.6	-0.5
F8	39.6	*f*		39.1	*f*	
F9	26.0	*f*		25.8	26.0	0.2
F10	124.1	126.1	2.0	124.0	124.1	0.1
F11	131.9	131.2	-0.7	131.0	130.4	-0.6
F12	25.3	*f*		25.2	25.8	0.6
F3′	16.1	*f*		16.0	15.0	-1.0
F7′	15.5	*f*		15.5	*f*	
F11′	17.2	*f*		17.2	*f*	

a The numbering is according to Figure 5.2. *b* Balaban *et al.* (1995). *c* This study *d* The 8^2 response could not be resolved from the 8^1 signal. *e* The signals for 17^1 and 17^2 are overlapping in the spectra. *f* Signals could not be resolved.

The 1D ^{15}N CP-MAS spectra for chlorosomes from the *bchQR* mutant and the WT are shown in Figures 5.4 and 5.5. A narrow signal for N-II is observed for both the mutant and the WT. The N-I and N-III signals have been assigned using data for BChl *c* in solution reported by Wang and co-workers [25]. The signals for N-I and N-III are well separated in the mutant, and the signal for N-III can additionally be decomposed into at least two components with approximate intensity ratios of 2:1. N-I and N-III overlap in the WT spectrum. The signal for N-IV splits into two well resolved peaks of almost equal intensity at 237.3 and 242.0 ppm for chlorosomes from the *bchQR* mutant, similar to what was observed for solid 17^2-farnesyl-*R*-[E,E] BChl *c* aggregates [26]. In the WT a broad response from 240 to 255 ppm is observed. Using Gaussian deconvolution, the N-IV response of the WT can be decomposed into three

overlapping components at 246.1, 248.9 and 254.2 ppm, with intensity ratios of 4.0:3.5:2.5. The ^{15}N chemical shifts have been listed in Table 5.4.

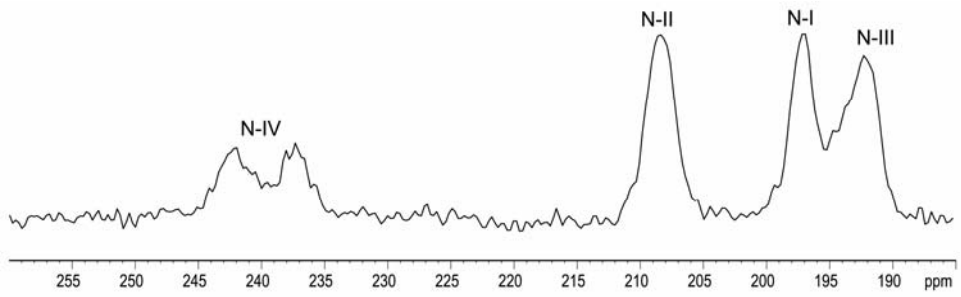

Figure 5.4 1D CP-MAS ^{15}N spectrum for uniformly ^{13}C, ^{15}N enriched chlorosomes from the *bchQR* mutant of *C. tepidum* recorded in a field of 17.6T at a 12 kHz MAS frequency is shown with a solid line. The CP contact time was set to 5.12 ms. 86,000 scans were accumulated with a recycle delay of 2 s. The dashed line spectrum is obtained by Gaussian deconvolution.

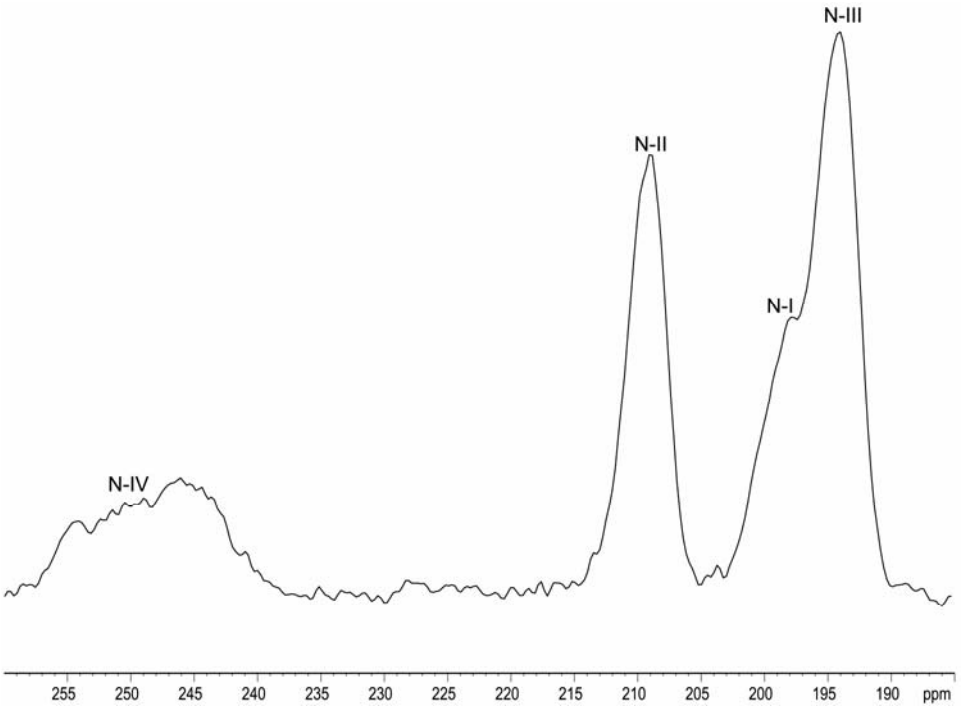

Figure 5.5 1D CP-MAS ^{15}N spectrum for uniformly ^{13}C, ^{15}N enriched chlorosomes from the WT of *C. tepidum* recorded in a field of 17.6T at a 12 kHz MAS frequency is shown with a solid line. The CP contact time was set to 5.12 ms. 86,000 scans were accumulated with a recycle delay of 2 s. The dashed line spectrum is obtained by Gaussian deconvolution.

Table 5.4 Assignments of ^{15}N chemical shifts of BChl *c* from the *bchQR* mutant and WT of *C. tepidum.*

Position	Monomer[a]	BChl *c* aggregates[b]		*bchQR*		WT	
		type A	type B	I	II	I	II
N-I	197.4	197.7	195.7	197.0		197.8	
N-II	209.7	209.8	208	208.4		209.0	
N-III	193.7	194.8		192.3	194.6	194.1	
N-IV	248.5	247.5	254.5	237.3	242.0	246.1	254.2

[a] Monomer shifts for (3^1*R*)-[*E*,*E*] BChl c_F in acetone-d_6[25,26]. [b] (3^1*R*)-[*E*,*E*] BChl c_F in solid aggregates treated in CH_2Cl_2 [26].

The ring-current effects for ^{15}N are more difficult to discern due to the paramagnetic shielding effects that reflect the details of the electronic environment and dominate the ^{15}N chemical shifts. The chemical shifts for N-I, N-II, and N-III are close to the reported shifts for the monomer in solution. However, the signals for N-IV in the *bchQR* mutant are shifted upfield with respect to the solution shifts by -11.2 and -6.5 ppm, while for the WT chlorosomes the stronger response is shifted by -2.4 ppm and the peak with less intensity is shifted downfield by +5.7 ppm.

5.3.2 Distance constraints

The correlations in Figure 5.6A that appear for a short CHHC mixing time of 250 μs are between nearby substituents of BChl *c* molecules in the mutant and represent ^1H-^1H distances of up to ~3.5 Å, in line with the proton transfer range previously published for this experiment [14,27,28]. These correlations represent intramolecular as well as intermolecular contacts which are indicated in Figure 5.6A in normal and bold type face respectively. The 7^1/18 and 7^1/18^1 cross peaks are significant since the possibilities for molecular assembly where these molecules are in close proximity is limited to the *syn-anti* structural modes, where these contacts represent intermolecular correlations within the stack. Intermolecular correlations between carbons 12^1/3^1, 12^1/2^1, and 12^1/3^2 are detected between rings I and III of two BChl *c* molecules from adjacent stacks. The 12^1/3^1 correlation is observed corresponding to both components of 3^1. This is attributed to the presence of two different conformations of the 3^1 side chain corresponding to the *syn* and *anti* orientations.

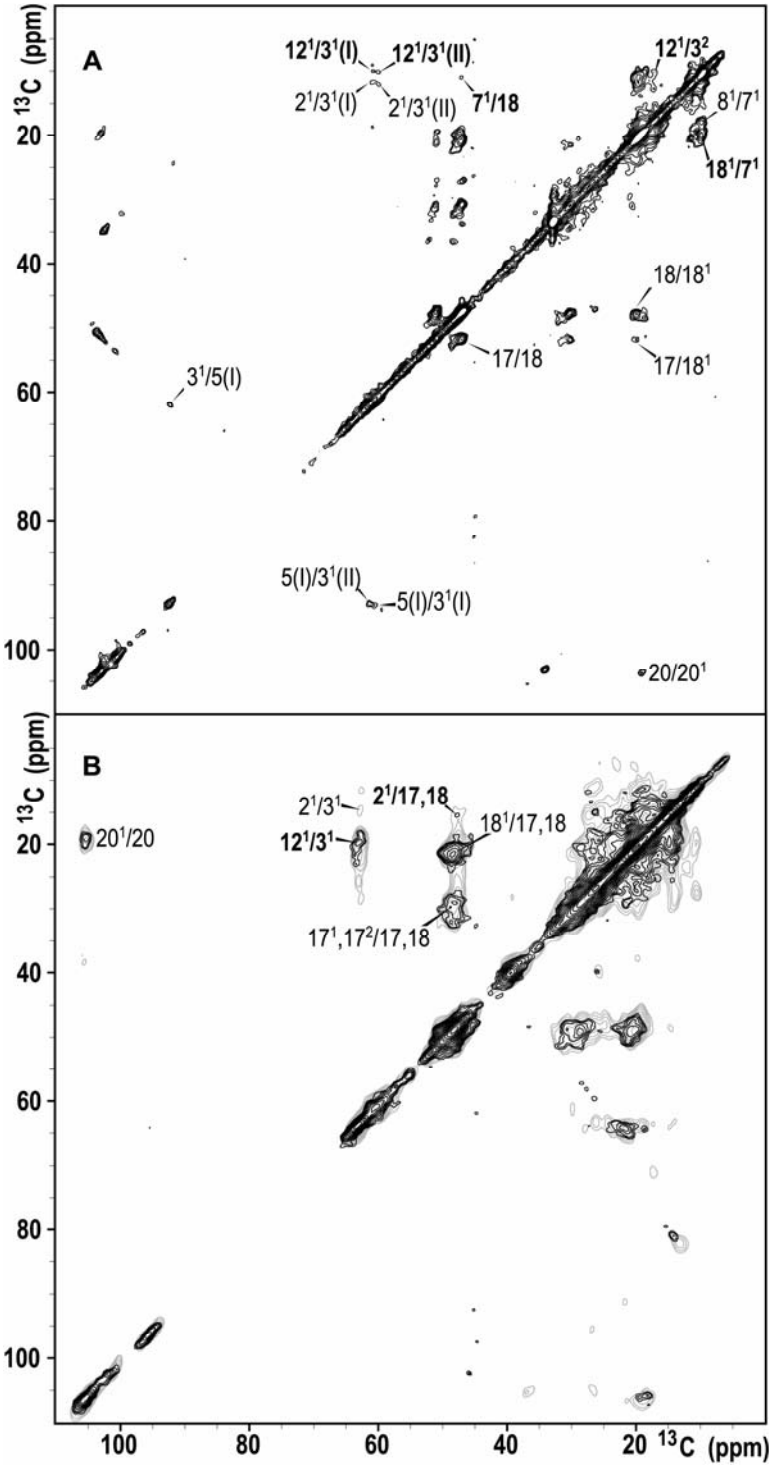

Figure 5.6 ^{13}C-^{13}C CHHC datasets of chlorosomes from the (A) *bchQR* mutant and (B) WT of *C. tepidum* recorded in a field of 17.6 T using spinning frequencies of 13 kHz. A ^{1}H-^{1}H spin diffusion mixing time of 250 µs is used for the *bchQR* mutant while mixing times of 300 µs (black spectrum) and 400 µs (grey spectrum) were employed for the WT. The correlations labeled in bold face are assigned as intermolecular.

Figure 5.6B shows an overlay of two CHHC datasets recorded for chlorosomes from the WT at mixing times of 300 and 400 μs in black and grey respectively. The $7^1/18$ and $7^1/18^1$ correlations, which determined the *syn-anti* stacking for the *bchQR*, are not resolved for the WT chlorosomes. In addition, the $12^1/3^2$ inter-stack cross-peak that is observed, for the *bchQR* mutant falls in the unresolved part of the spectrum near the diagonal in the WT, though the $12^1/3^1$ inter-stack contact is observed. A new correlation is observed in the WT datasets, which has tentatively been assigned as intermolecular to $2^1/17,18$ (17 and 18 are very close in chemical shift) based on the chemical shift values. This correlation is would fit in an all *syn* or all *anti* coordinated parallel stacking framework [7,10,29].

5.3.3 Ring deformation

In order to evaluate the effects of *syn* and *anti* coordination on the out-of-plane ring deformation, two geometry optimized molecules of 17^2-methyl-*R*-[E,M] BChl *c*, of which one was *syn* coordinated and the other *anti* coordinated to a methanol molecule, was processed with the NSD program to calculate the out-of-plane ring deformations in the lowest frequency modes (Table 5.5) [8]. The *anti* coordinated BChl *c* shows a pronounced saddling with additional doming and ruffling displacement. The *syn* coordinated BChl *c* shows less overall displacement than for the *anti* coordinated molecule, especially for the ruffling component.

Out-of-plane distortions have an effect on the metal-nitrogen separation [8]. *Ab initio* quantum chemical calculations and solid-state NMR studies on metal-tetraphenylporphyrin compounds indicate that the ^{15}N chemical shifts tend to be determined by the metal-nitrogen separation [30]. As a result the observed out-of-plane displacements can be broadly correlated to the doubling seen for the ^{15}N chemical shifts of N-IV. In Table 5.5 the overall distortion of 17^2-methyl-*R*-[E,M] BChl *c* that is *anti* coordinated differs from the *syn* coordinated BChl *c* molecule by ~0.2 Å. The data indicate that the chlorosomes from the *bchQR* mutant have the *syn-anti* building block for stack formation, implying that half the BChl *c* molecules are *syn* coordinated and the other half are *anti* coordinated. The two distinct N-IV peaks of almost equal intensity seen for the *bchQR* mutant

that comprises of only 17^2-farnesyl-*R*-[E,M] BChl *c* molecules can be reconciled with the presence of equal amounts of *syn* and *anti* coordinated BChl *c*. Reduced saddling and ruffling is observed for syn-BChl *c* when compared to *anti*-BChl *c*. The broad response seen for N-IV in the WT chlorosomes is more difficult to generalize because of the presence bulkier groups at 8-C and 12-C. The intensity ratio of the N-IV peaks in the WT chlorosomes is seen to be 4:3.5:2.5, which suggests that ring deformation is determined by more than one factor, such as the different side chains present at 8-C and 12-C positions.

Table 5.5 Out-of-plane (Å) distortions of the in the lowest frequency mode for geometry optimized structures of non-coordinated, 3^1 –R *syn*-coordinated and *anti*-coordinated [E,M] BChl *c* using Normal-Coordinate Structural Decomposition. The observed total distortions (d_{obs}) as well as the corresponding standard deviation (δ) are also listed.

BChl *c*	*Out-of-plane displacements (Å)*							
	total distortion		B_{2u}	B_{1u}	A_{2u}	$E_g(x)$	$E_g(y)$	A_{1u}
	d_{obs}	δ	d_{sad}	d_{ruf}	d_{dom}	$d_{wav(x)}$	$d_{wav(y)}$	d_{pro}
anti	1.723	0.220	1.094	0.814	0.871	-0.069	0.296	-0.509
syn	1.503	0.183	0.893	0.459	0.701	-0.287	0.481	-0.667

5.3.4 Spectral doubling

To trace the source of the doubling observed in the NMR datasets of the chlorosomes from the *bchQR* mutant, additional calculations were done. To determine the basic difference in ^{13}C and ^{15}N chemical shifts between the *syn*-BChl *c* and the *anti*-BChl *c*, two 17^2-methyl-*R*-[E,M] BChl *c* monomers, one *syn* coordinated and the other *anti* coordinated to a methanol molecule were optimized quantum mechanically. Their ^{13}C chemical shifts were calculated using the same DFT method as is described in Chapter 4. The difference in their chemical shifts is plotted as dashed circles in Figure 5.7. The spectral doublings seen at positions 17-C, 19-C, and 20-C can arise in part from basic differences in ring distortion originating from *syn* and *anti* coordination for chlorosomes from the *bchQR* mutant, but there are other, as yet unknown, effects as well. It can be seen from Table 5.5 that the overall distortion of a BChl *c* that is *anti* coordinated differs from a *syn* coordinated BChl *c* molecule by ~0.2 Å.

This is consistent with the doubling around ring IV seen for chlorosomes from the *bchQR* mutant, which can be attributed to the presence of both *syn* and *anti* coordinated molecules in the basic building block.

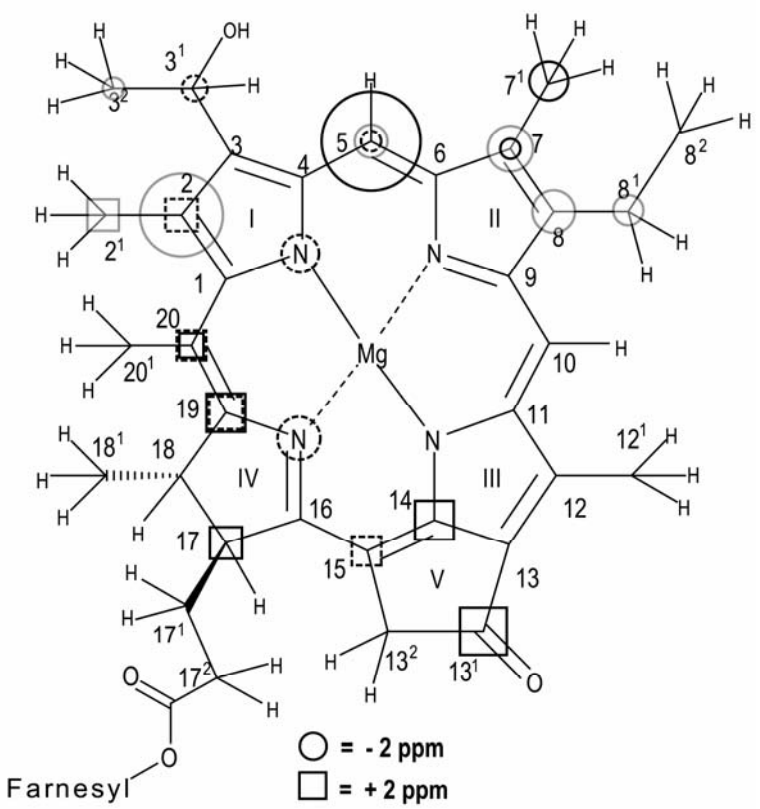

Figure 5.7 The differences in the calculated chemical shifts of geometry optimized *syn* and *anti* coordinated BChl *c* monomers are plotted as dashed circles/squares, while the differences between *syn* and *anti* BChl *c* molecules taken from a six *syn-anti* stack optimized aggregate are plotted as grey circles/squares. The experimental difference between components I and II for the *bchQR* mutant are shown as solid circles/squares. Differences for > |±1.5| ppm are indicated. The sizes of the circles and squares are proportional to the magnitude of the shift.

When BChl *c* molecules are in a *syn-anti* stack, the 3^1 side chain has alternating molecular conformations from one *syn* coordinated molecule to the next *anti* one within the stack, to be able to form the coordinate bond with the adjacent molecule. This difference in conformation could have an effect on the chemical shifts of atoms in the vicinity of 3^1, specifically at the 5 and 2^1 positions. To determine the effect of this rotation on the chemical shift a set of six *syn-anti* stacks, each stack comprising twelve

BChl *c* molecules, was optimized using molecular mechanics, with the MM+ force field in Hyperchem 7. From the central part of this six stack aggregate, *syn* and *anti* ligated BChl *c* molecules were selected and their chemical shifts were individually calculated. The difference in the calculated *syn* and *anti* shifts in an aggregate are plotted as grey circles in Figure 5.7, where the radius of the circle/square is proportional to the magnitude of the shift. Interestingly, in addition to the expected chemical shift differences observed for the calculation at positions 5-C, 2-C, and 2^1-C, differences also arise at positions 7-C, 8-C, and 8^1-C in ring II.

5.3.5 Structural assessment: Mutant vs. WT

The Q_y absorption band of the *bchQR* mutant has a half-band width that is much less than for the WT [2]. This limits the range of available wavelengths of light in the far-red region that can be utilized by the mutant, thereby drastically reducing its light-harvesting potential [2]. This emphasizes the role that the degree of methylation at the 8^2-C and 12^1-C plays in steering the self-assembly in chlorosomes so as to form higher aggregates with an increased light-harvesting capacity [4,5]. Studies on *in vitro* aggregates of BChls *c* have shown that varying degrees of methylation at 8^2 and 12^1 and the stereoisomeric configuration at 3^1 influence the structure of the aggregates [4,31-34]. Gomez *et al.* have shown that the absorption spectrum of the *bchQR* double mutant cells which produce 17^2-farnesyl-*R*-[E,M] BChl *c* varies from that of the related *bchQ* single mutant which produces mostly 17^2-farnesyl-*R*-[E,E] BChl *c*, suggesting that the aggregates of [E,M]-BChl *c* may structurally differ from those of [E,E]-BChl *c* in the mutant chlorosomes [2]. This is consistent with dissimilarities in the chemical shift and aggregation shift patterns that we have observed between chlorosomes from the *bchQR* mutant which contain only [E,M] BChl *c* and the WT, which contains ~ 80% of [Pr,E]/[E,E] BChl *c*. This has led me to assess their structures independently. The distance constraints collected for chlorosomes from the *bchQR* mutant favor a *syn-anti* stacked model, similar to what has been resolved for the *bchQRU* mutant chlorosomes.

As has been described in Chapter 4, the clear 1.25 nm layer line observed for the WT is indicative of a the repeat of a pair of BChl

molecules along the stack. Hence in the WT the there is no possibility of forming all *anti* coordinated or all *syn* coordinated stacks, since this would be in violation of the structural restraint imposed by the EM data. For the WT, the model built with parallel stacks having the *syn-anti* based structural unit, as has been observed for the mutants still remains the one which is consistent with the EM data. In this scheme, the doubling around position 7^1 could be due to presence of different [Pr,E] and [E,E] homologues, which are known to produce different structures [35]. The doubling observed at position 5 could possibly be caused by the alternating conformation of the 3^1 side chain when going from a *syn* to an *anti* coordinated molecule in the stack.

5.4 Conclusions

Solid state NMR data suggest that the chlorosomes from the *bchQR* mutant of *C. tepidum*, which produces chlorosomes with only 17^2-farnesyl-*R*-[E,M] BChl *c* are also made up of parallel stacks with the *syn-anti* building block. For chlorosomes from the WT though distance constraints cannot be resolved, structural constraints from EM corresponding to a dimeric repeat along the stack favor a *syn-anti* based microstructure for these chlorosomes.

References

[1] A. G. M. Chew and D. A. Bryant (**2007**) *Annual Review of Microbiology* 61: 113-129.

[2] A. G. M. Chew, N. U. Frigaard and D. A. Bryant (**2007**) *Journal of Bacteriology* 189: 6176-6184.

[3] G. T. Oostergetel, M. Reus, A. G. M. Chew, D. A. Bryant, E. Boekema and A. R. Holzwarth (**2007**) *FEBS Letters* 581: 5435-5439.

[4] T. Ishii, M. Kimura, T. Yamamoto, M. Kirihata and K. Uehara (**2000**) *Photochemistry and Photobiology* 71: 567-573.

[5] N. U. Frigaard and D. A. Bryant (**2006**) *Microbiology Monographs* 2: 79.

[6] S. Ganapathy, M. Reus, A. G. M. Chew, D. A. Bryant, A. R. Holzwarth and H. J. M. de Groot (**2007**) in: *Photosynthesis. Energy of Sun: 14th International Congress on Photosynthesis Research*: pp. 251-254 (J.F. Allen, Ed.) Springer, Glasgow.

[7] B. J. van Rossum, D. B. Steensgaard, F. M. Mulder, G. J. Boender, K. Schaffner, A. R. Holzwarth and H. J. M. de Groot (**2001**) *Biochemistry* 40: 1587-1595.

[8] W. Jentzen, X. Z. Song and J. A. Shelnutt (**1997**) *Journal of Physical Chemistry B* 101: 1684-1699.

[9] J. A. Shelnutt, X. Z. Song, J. G. Ma, S. L. Jia, W. Jentzen and C. J. Medforth (**1998**) *Chemical Society Reviews* 27: 31-41.

[10] T. S. Balaban, A. R. Holzwarth, K. Schaffner, G. J. Boender and H. J. M. de Groot (**1995**) *Biochemistry* 34: 15259-15266.

[11] A. E. Bennett, J. H. Ok, R. G. Griffin and S. Vega (**1992**) *Journal of Chemical Physics* 96: 8624-8627.

[12] A. Bielecki, A. C. Kolbert and M. H. Levitt (**1989**) *Chemical Physics Letters* 155: 341-346.

[13] B. J. van Rossum, H. Förster and H. J. M. de Groot (**1997**) *Journal of Magnetic Resonance* 124: 516-519.

[14] I. de Boer, L. Bosman, J. Raap, H. Oschkinat and H. J. M. de Groot (**2002**) *Journal of Magnetic Resonance* 157: 286-291.

[15] M. J. Frisch et al. (**2004**) Gaussian, Inc., Wallingford CT.

[16] A. D. Becke (**1986**) *Journal of Chemical Physics* 84: 4524-4529.

[17] C. T. Lee, W. T. Yang and R. G. Parr (**1988**) *Physical Review B* 37: 785-789.

[18] J. C. Facelli (**1998**) *Journal of Physical Chemistry B* 102: 2111-2116.

[19] Z. F. Chen, C. S. Wannere, C. Corminboeuf, R. Puchta and P. V. Schleyer (**2005**) *Chemical Reviews* 105: 3842-3888.

[20] R. Ditchfield (**1972**) *Journal of Chemical Physics* 56: 5688-5691.

[21] K. Wolinski, J. F. Hinton and P. Pulay (**1990**) *Journal of the American Chemical Society* 112: 8251-8260.

[22] R. Ditchfield (**1974**) *Molecular Physics* 27: 789-807.

[23] G. J. Boender (**1996**) *PhD Thesis,* Leiden University.

[24] R. J. Abraham and A. E. Rowan (**1991**) *Nuclear magnetic resonance spectroscopy of chlorophyll*, (H. Scheer, Eds.) CRC Press, Boca Raton FL.

[25] Z. Y. Wang, M. Umetsu, M. Kobayashi and T. Nozawa (**1999**) *Journal of the American Chemical Society* 121: 9363-9369.

[26] M. Umetsu, J. G. Hollander, J. Matysik, Z. Y. Wang, T. Adschiri, T. Nozawa and H. J. M. de Groot (**2004**) *Journal of Physical Chemistry B* 108: 2726-2734.

[27] A. Lange, K. Seidel, L. Verdier, S. Luca and M. Baldus (**2003**) *Journal of the American Chemical Society* 125: 12640-12648.

[28] S. Ganapathy, A. J. van Gammeren, F. B. Hulsbergen and H. J. M. de Groot (**2007**) *Journal of the American Chemical Society* 129: 1504-1505.

[29] A. R. Holzwarth and K. Schaffner (**1994**) *Photosynthesis Research* 41: 225-233.

[30] M. Strohmeier, A. M. Orendt, J. C. Facelli, M. S. Solum, R. J. Pugmire, R. W. Parry and D. M. Grant (**1997**) *Journal of the American Chemical Society* 119: 7114-7120.

[31] T. S. Balaban, A. R. Holzwarth and K. Schaffner (**1995**) *Journal of Molecular Structure* 349: 183-186.

[32] J. Chiefari, K. Griebenow, N. Griebenow, T. S. Balaban, A. R. Holzwarth and K. Schaffner (**1995**) *Journal of Physical Chemistry* 99: 1357-1365.

[33] T. Mizoguchi, K. Hara, H. Nagae and Y. Koyama (**2000**) *Photochemistry and Photobiology* 71: 596-609.

[34] Y. Saga, K. Matsuura and H. Tamiaki (**2001**) *Photochemistry and Photobiology* 74: 72-80.

[35] J. R. Diers, Y. W. Zhu, R. E. Blankenship and D. F. Bocian (**1996**) *Journal of Physical Chemistry* 100: 8573-8579.